

Graphene-InSe-graphene van der Waals heterostructures

S. A. Svatek¹, G. W. Mudd¹, Z. R. Kudrynskyi¹, O. Makarovsky¹, Z. D. Kovalyuk², C. J. Mellor¹, L. Eaves¹, P. H. Beton¹, and A. Patané¹

¹ School of Physics and Astronomy, The University of Nottingham, Nottingham, NG7 2RD (UK)

² Institute for Problems of Materials Science, The National Academy of Sciences of Ukraine, Chernivtsi, 58001 (Ukraine)

amalia.patanè@nottingham.ac.uk

Abstract. We exploit the broad-band transparency of graphene and the favorable energy band line-up of graphene with *n*-type InSe thin films to create graphene-InSe-graphene heterostructures with high photosensitivity at room temperature. We use a semiclassical model to describe the photoresponse and its dependence on the electron transit time through the InSe layer.

1. Introduction

Van der Waals (vdW) heterostructures are made by stacking thin exfoliated layers of two-dimensional crystals such as graphene, hexagonal boron nitride, and the transition metal dichalcogenides [1-2]. Because the component layers are held together by weak van der Waals forces, both the structural integrity and the electronic and optical properties of the individual atomic planes are maintained. These new materials are not only of fundamental interest, but have the potential for exploitation in novel electronic and optoelectronic devices.

Here we present vdW crystalline heterostructures based on graphene and the direct-band gap metal chalcogenide InSe, an exfoliable and stable semiconductor that extends the current library of vdW crystals. Recent reports of bendable photodetectors [3], large-scale image sensors [4], *p-n* LED junctions [5], and FETs [6] have demonstrated the potential of InSe for future technologies. In particular, our recent work [7] on graphene/InSe heterostructures has demonstrated that the weak optical absorbance of graphene makes this single atomic carbon layer a particularly attractive option for use as a transparent electrical contact compared to conventional metals [8]. Furthermore, the work function of graphene can be adjusted by the electric field effect, an important feature for adjustable band alignment at the interface with a vdW crystal.

We focus on a device architecture where the InSe and two graphene layers are “vertically” stacked. In this graphene/InSe/graphene heterostructure, the small separation (~ 100 nm) between the graphene electrodes leads to a short transit time for the electrons photogenerated in the optically active InSe, thus enabling high photoresponsivity at room temperature.

2. Samples and device fabrication

Our γ -InSe crystals were grown using the Bridgman method from a polycrystalline melt of $\text{In}_{1.03}\text{Se}_{0.97}$. The primitive unit cell contains three InSe layers each of which has a thickness of 8.320 Å and



consists of four covalently bonded monoatomic sheets in the sequence Se-In-In-Se; along the c -axis, the primitive unit cell has a lattice constant of $c = 24.961 \text{ \AA}$ and, within each a - b plane, atoms form hexagons with lattice parameter $a = 4.002 \text{ \AA}$ (Figure 1). In its bulk form, InSe is a semiconductor with direct band gap energy ($E_g = 1.26 \text{ eV}$ at $T = 300\text{K}$) that can be increased due to quantum confinement by reducing the number of layers in the crystalline sheet [9]; also, InSe contains native donors due to In-interstitial atoms [10] and it retains a relatively high electron mobility (10^{-2} - $10^{-1} \text{ m}^2/\text{Vs}$) [8] over an extended range of InSe thicknesses down to a few nanometers ($\sim 10 \text{ nm}$).

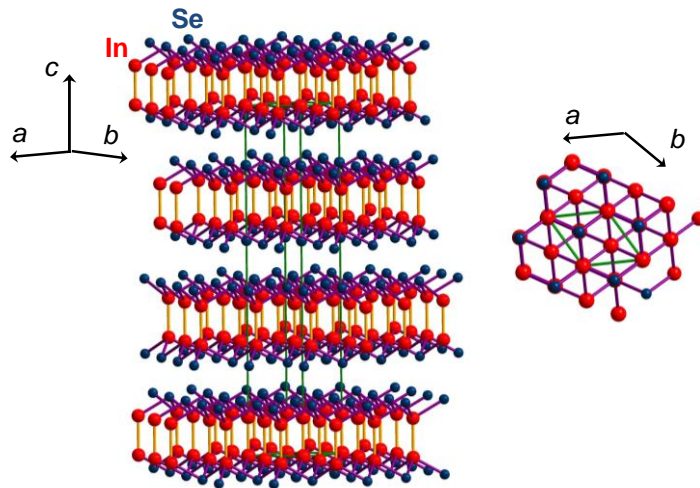


Figure 1. Crystal structure of γ -InSe van der Waals crystals.

The graphene/ n -InSe/graphene heterostructures were fabricated using large area CVD graphene grown on copper. The main steps in the fabrication of these heterostructures are shown in Figure 2 and differ from those previously used to form vertical tunnel devices with exfoliated graphene [11].

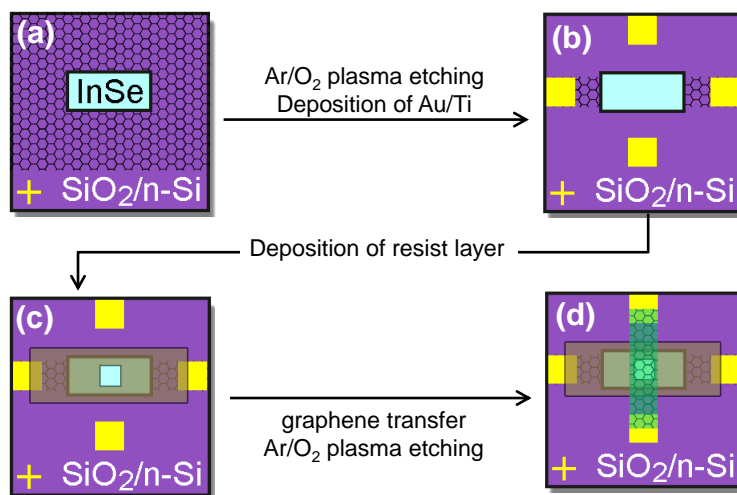


Figure 2. Main steps in the fabrication of graphene/ n -InSe/graphene heterostructures.

a) An InSe flake is deposited on CVD graphene.
b) The graphene layer is patterned and etched to leave a graphene strip under the InSe flake. Au/Ti contact pads are then deposited.
c) An isolation layer, AR-N, is formed to cover the InSe flake and the lower graphene contact. A window is formed in the AR-N layer on the surface of the InSe.
d) The top graphene contact strip is defined by etching.

In our approach, following deposition of Au/Ti alignment marks on a SiO_2/Si substrate (SiO_2 layer thickness of 300 nm), CVD graphene was transferred by a wet transfer technique and cleaned. InSe flakes were deposited by exfoliation and a flake of thickness t was selected using optical microscopy (Figure 2a). The graphene layer was patterned and etched in an Ar/O_2 plasma to leave a graphene strip, which provided a continuous connection to the bottom of the InSe flake. Au/Ti contact pads ($110 \text{ nm}/15 \text{ nm}$) were then deposited at each end of the lower contact strip. In the same step Au/Ti pads were also formed to provide contacts to the upper graphene strip, which was deposited in a later

fabrication step (Figure 2b). An isolation layer was then formed by exposing a negative resist, AR-N, using electron beam lithography; this covered the lower graphene contact including the edges of the InSe flake, to avoid the formation of electrical shorts between upper and lower graphene strips. A window with an area of approximately $2\ \mu\text{m} \times 2\ \mu\text{m}$ was formed in the AR-N layer on the top surface of the InSe to facilitate the mechanical contact with the upper graphene layer (Figure 2c). Finally, a second layer of graphene was transferred; in this case the supporting PMMA film, which was added to the graphene/copper before etching in FeCl_3 , was not removed, but instead used as the resist layer in a further stage of electron beam lithography in which the upper graphene contact strip was defined by etching in an Ar/O_2 plasma. The resulting upper contact runs at right angles to the lower strip to form a graphene/*n*-InSe/graphene vertical heterostructure and overlaps the Au/Ti contacts formed at an earlier stage of the process (see Figure 2d).

3. Results and discussion

Figure 3a illustrates the schematic layered structure and an optical image of a graphene-*n*-InSe-graphene device. Here the top- (g_1) and bottom-graphene (g_2) layers overlap an InSe nanoflake of thickness $t = 130\ \text{nm}$ and serve as source and drain to the InSe conducting channel. As shown in Figure 3b, the dependence of the dark current, I , on the bias voltage, V_s , applied between the two graphene electrodes is non-linear. A non-linear V_s -dependence is also observed for the photocurrent ΔI (Figure 3c).

The non-linearity and asymmetry of the current-voltage characteristics is not observed in planar graphene-*n*-InSe-graphene devices [7] and may arise from a spurious contact resistance at the InSe/graphene interface caused by surface defects introduced during the fabrication process. In fact, the upper contact to InSe is formed through mechanical transfer of CVD graphene onto a hole within an isolation layer (AR-N), which is formed from a negative resist. In this case the top InSe surface is coated with resist, which is subsequently removed during the development process. In addition, the upper graphene layer is transferred by floating the PMMA/graphene on water after a cleaning cycle, and then submerging the target substrate under the PMMA/graphene in order to scoop it up. In this process there is scope for residual resist layers to remain on the InSe surface; also, the InSe layer is immersed in water; both these processes may compromise the top graphene/InSe interface. Nevertheless, the implementation of these fabrication processes to realize a working vdW heterostructure device represents significant progress and offers a route to the device scalability using large area CVD graphene.

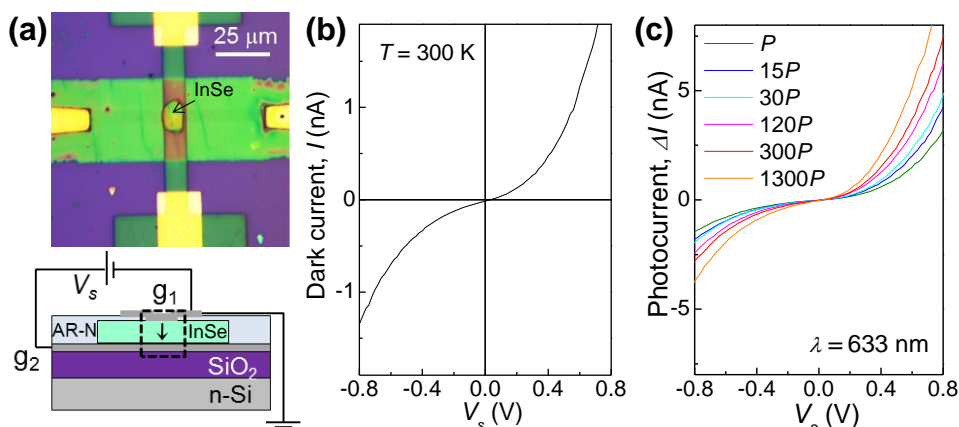


Figure 3. a) Schematic structure and optical image of a graphene-*n*-InSe-graphene vertical device. The graphene layers, g_1 and g_2 , are separated by an InSe flake of thickness $t = 130\ \text{nm}$. b) Dark current, I , and c) photocurrent, ΔI , versus applied bias V_s at $T = 300\ \text{K}$. The photocurrent is measured with a laser beam of wavelength $\lambda = 633\ \text{nm}$ ($P = 10^{-13}\ \text{W}$).

As shown in Figure 4, our heterostructure exhibits a stable and reproducible photoresponsivity R with values of up to 10^4 A/W at $\lambda = 633$ nm and $V_s = 1$ V, and response to light at powers P as low as $\sim 10^{-13}$ W over an area of the InSe flake of $\sim 4 \mu\text{m}^2$. Also, a power law relation of the form $R = CP^n$, with $n = 2/3$ where C is a constant, provides a good empirical fit to the data (see lines in Figure 4).

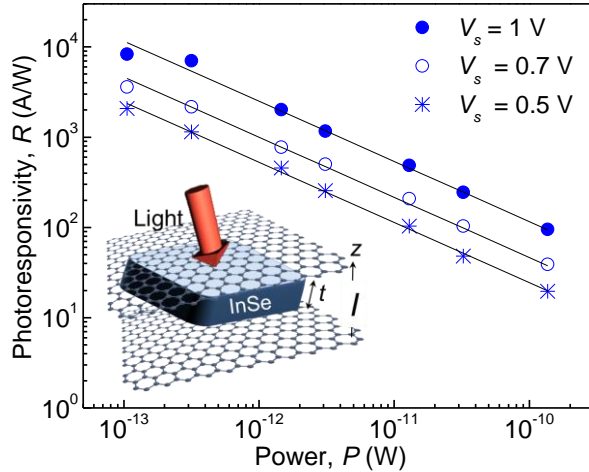


Figure 4. Photoresponsivity versus laser power at $T = 300$ K and $\lambda = 633$ nm, and various applied voltages V_s . The lines describe the empirical power law, i.e. $R = CP^n$, where $n = 2/3$ and C is a constant that depends on the applied voltage V_s .

To model the photoresponsivity, we consider an n -type InSe channel of width w , thickness t , and length l , with ohmic (graphene) contacts across its thickness t (inset of Figure 4). When light of power P and energy $h\nu$ larger than the band gap energy of InSe falls on the surface of the InSe flake, electron-hole pairs are generated. The densities of photo-created electrons and holes are equal and, at steady state, they can be expressed in terms of the minority carrier (hole) lifetime, τ_i , and the rate of carrier generation by light G , i.e. $\Delta n = \Delta p = G\tau_i$ [12], where $G = (t\alpha P/h\nu)(wtl)^{-1}$ and α is the absorption coefficient of InSe at the energy $h\nu$. Since the mobility μ of electrons is much larger than that of holes, we express the photocurrent ΔI in terms of the dominant electron current, $\Delta I = \Delta n e v_d w l$, where $v_d = t/\tau_i$ is the electron drift velocity and τ_i is the electron transit time across an InSe channel of thickness t . Thus we can express ΔI as

$$\Delta I = (et\alpha P/h\nu)(\tau_i/t), \quad (1)$$

from which we derive the photoresponsivity R , the external quantum efficiency EQE , and the internal quantum efficiency IQE :

$$R = \Delta I/P = (et\alpha/h\nu)(\tau_i/t), \quad (2)$$

$$EQE = R(h\nu/e) = (t\alpha)(\tau_i/t), \quad (3)$$

$$IQE = EQE/t\alpha = \tau_i/t. \quad (4)$$

From equations 2-4, it can be seen that R , EQE , and IQE are all proportional to the ratio between the minority carrier lifetime and electron transit time, τ_i/t . In particular, a small separation t between the graphene electrodes and/or a larger applied bias V_s should lead to a faster electron transit time, $\tau_i = t^2/\mu V_s$, and hence larger values of R , EQE ($\sim V_s/t$) and IQE ($\sim V_s/t^2$). For $V_s = 1$ V, $t = 130$ nm and an electron mobility $\mu = 0.1 \text{ m}^2\text{V}^{-1}\text{s}^{-1}$, we estimate an electron transit time $\tau_i \sim 1.7 \times 10^{-13}$ s. Thus a value of

$R \sim 10^4$ A/W, measured at the lowest incident power P , corresponds to $\tau_i/\tau_r \sim 1.5 \times 10^5$ and $\tau_i \sim 2.6 \times 10^{-8}$ s for $\alpha = 10^6$ m⁻¹ at $h\nu = 1.96$ eV.

As shown in Figure 4, the photoresponsivity depends on the optical power P . The measured decrease of R with increasing P suggests a decrease of τ_i and/or an increase of τ_r . The transit time of photo-induced carriers may be increased by the power due to enhanced scattering. Also, an increasing power can induce Auger recombination processes and increases the carrier recombination rate, thus reducing the carrier lifetime τ_i .

The measured photoresponsivity is significantly larger than that reported for photodetectors based on graphene and/or vdW 2D crystals at similar wavelengths and laser powers, which do not exceed values of 10^3 A/W [13]. Also, we note that although a higher photoresponsivity can be achieved in phototransistors based on graphene and colloidal nanocrystals [14], the performance of such hybrid photodetectors tends to be compromised by a slow (~ 1 s) optical response due to the slow escape rate of photogenerated charges confined in the nanocrystals. In contrast, for our structures, the mechanism responsible for the photoresponse does not rely on a charge trapping effect as light generates free carriers. These features of our heterostructures enable a modulation of the dark and photocurrent at shorter (\sim ms- μ s) time scales.

4. Conclusion

In summary, our findings demonstrate that mechanically formed heterojunctions of InSe and graphene have optical and electrical properties with potential for applications in optoelectronics. Our innovative fabrication methods could be extended to other material systems and device architectures. It should be possible to achieve different band alignments by combining InSe with other layered crystals, such as semiconducting gallium and indium chalcogenides (*e.g.* InX and GaX, where X = S, Se, Te). These layered semiconductors have direct band-gaps covering a wide wavelength range from the visible to the near-infra-red (NIR) (0.5-1 μ m), and provide a class of 2D compounds for versatile band-gap engineering. In combination with transparent, conducting graphene, these new heterostructures could be used to create miniaturized device structures for 2D electronics and optoelectronics compatible with a wide variety of materials including dielectric, polymer and flexible substrates.

Acknowledgements

We thank Neil Wilson and Alex Marsden (Department of Physics, Warwick University) for the graphene grown by CVD, which was used in these studies. This work was supported by the Engineering and Physical Sciences Research Council (EPSRC), the National Academy of Sciences of Ukraine, and the EU Graphene Flagship Programme.

References

- [1] A. K. Geim, I. V. Grigorieva, *Nature* 2013 **499**, 419-425.
- [2] A.C. Ferrari et al., *Nanoscale* 2015, **7**, 4598.
- [3] R. T. Srinivasa et al., *Nano Lett.* 2014, **14**, 2800.
- [4] S. Lei et al., *Nano Lett.* 2015, **15**, 259.
- [5] N. Balakrishnan et al., *Adv. Opt. Mater.* 2014, **2**, 1064.
- [6] W. Feng, W. Zheng, W. Cao, and P. A. Hu, *Adv. Mater.* 2014, **26**, 6587.
- [7] G.W. Mudd et al., *Adv. Materials* 2015, DOI: 10.1002/adma.201500889.
- [8] W. Feng, X. Zhou, W. Q. Tian, W. Zheng, and P.A. Hu, *Phys. Chem. Chem. Phys.* 2015, **17**, 3653.
- [9] G.W. Mudd et al., *Adv. Materials* 2013, **25**, 5714.
- [10] G.W. Mudd et al., *Appl. Phys. Lett.* 2014, **105**, 221909.
- [11] C. R. Dean et al., *Nature* 2013, **497**, 598.
- [12] S.M. Sze, *Semiconductor devices, Physics and Technology*, 2nd edition, pages 61-62.
- [13] F. Xia, H. Wang, D. Xiao, M. Dubey, and A. Ramasubramaniam, *Nat. Photon.* 2014, **8**, 899.
- [14] L. Turyanska et al., *Adv. Electr. Mat.* 2015, DOI: 10.1002/aelm.201500062.